# Precise Creation, Characterization, and Manipulation of Single Optical Qubits

Nicholas Peters, Joseph Altepeter, Evan Jeffrey, David Branning, and Paul Kwiat

*Department of Physics, University of Illinois, 1110 W. Green St.*
*Urbana, Illinois 61801,USA*

Received June 28, 2003
Revised September 16, 2003

We present the theoretical basis for and experimental verification of arbitrary single-qubit state generation, using the polarization of photons generated via spontaneous parametric downconversion. Our precision measurement and state reconstruction system has the capability to distinguish over 3 million states, all of which can be reproducibly generated using our state creation apparatus. In order to complete the triumvirate of single qubit control, there must be a way to not only manipulate single qubits after creation and before measurement, but a way to characterize the manipulations *themselves*. We present a general representation of arbitrary processes, and experimental techniques for generating a variety of single qubit manipulations, including unitary, decohering, and (partially) polarizing operations.

*Keywords*: photon polarization, qubit, quantum process, tomography, parametric downconversion
*Communicated by*: J Shapiro & H-K Lo

## 1 Introduction

Quantum information processing (QIP) promises great potential power over its classical counterpart in the areas of computing, communication, and metrology [1]. Nearly all QIP protocols require specific initial states and the ability to manipulate the qubits with exquisite precision. Here we demonstrate the creation of arbitrary single qubit states encoded in the polarization of single photons. Single-photon Fock states are conditionally realized by detecting one photon of a pair produced in the process of spontaneous parametric downconversion [2]. We manipulate the photons' polarization state using a series of birefringent waveplates (which enable any unitary transformation) and a thick birefringent decoherer (which allows the production of mixed states). Using a method of state tomography, we can experimentally determine the most likely density matrix which describes the resulting quantum state. Finally, we have implemented several versions of *process* tomography, by which we can accurately characterize

any quantum process acting on the polarization qubit, including all unitary transformations, (partial) measurements, and decoherence.

## 2 State Creation

We represent our qubits by single-photon polarization states in the horizontal-vertical basis, with the state vectors

$$|0\rangle \equiv |H\rangle \equiv \begin{pmatrix} 1 \\ 0 \end{pmatrix} \text{ and } |1\rangle \equiv |V\rangle \equiv \begin{pmatrix} 0 \\ 1 \end{pmatrix}, \tag{1}$$

or in density matrix notation,

$$\rho_H = \begin{pmatrix} 1 & 0 \\ 0 & 0 \end{pmatrix} \text{ and } \rho_V = \begin{pmatrix} 0 & 0 \\ 0 & 1 \end{pmatrix}. \tag{2}$$

The density matrix of an arbitrary single qubit can be represented by three independent real parameters ($A$, $B$, and $\delta$):

$$\rho = \begin{pmatrix} A & Be^{i\delta} \\ Be^{-i\delta} & 1-A \end{pmatrix}, \tag{3}$$

where $0 \leq$ A $\leq 1$ from normalization, and $|B| \leq \sqrt{A(1-A)}$ from positive semi-definiteness. Another equivalent representation is given by

$$\rho = \frac{1}{2}(\mathbf{I} + \vec{\mathbf{r}} \cdot \sigma), \tag{4}$$

where $\mathbf{I}$ is the identity and we define the polarization analogs of the Pauli spin matrices as

$$\sigma_1 \equiv \begin{pmatrix} 0 & 1 \\ 1 & 0 \end{pmatrix}, \ \sigma_2 \equiv \begin{pmatrix} 0 & -i \\ i & 0 \end{pmatrix}, \text{ and } \sigma_3 \equiv \begin{pmatrix} 1 & 0 \\ 0 & -1 \end{pmatrix}. \tag{5}$$

The components of $\vec{\mathbf{r}}$ give the degree of polarization for the photon in the Horizontal-Vertical (H-V), Diagonal-Antidiagonal (D-A), and Right-Left Circular (R-L) bases.[a] As such, they are often identified as $r_H \equiv r_1$, $r_D \equiv r_2$, $r_R \equiv r_3$.[b] It is useful to view these components as coordinates in a 3-D space of polarizations; the constraint $|\vec{\mathbf{r}}| \leq 1$ implies that all states must lie inside or on a sphere of unit radius, known as the Poincaré sphere. Points on the *surface* of the sphere ($|\vec{\mathbf{r}}| = 1$) represent pure polarization states (linear polarization states on the equator, right and left circular polarization on the north and south pole, respectively), while points inside the surface ($|\vec{\mathbf{r}}| < 1$) represent partially mixed states. The center of the sphere ($|\vec{\mathbf{r}}| = 0$) corresponds to a completely mixed state, i.e., an unpolarized photon.

Because an arbitrary state has three independent parameters, the generation of such a state requires three adjustable elements. Considering the Poincaré sphere, we make an ansatz that a half-waveplate (HWP), followed by a thick birefringent decoherer, a half-waveplate, and a quarter-waveplate (QWP) are sufficient to generate all one-qubit polarization states from a pure linear polarization fiducial state ($|H\rangle$ in our case). We now derive formulae that

[a] These components $r_i$ are related to the Stokes parameters ($S_i$) of classical optics [3] by $r_i = \frac{S_i}{S_0}$.

[b] The conversion between the representations in 3 and 4 is given by $r_H = 2A - 1$, $r_D = 2B\cos(\delta)$, and $r_R = 2B\sin(\delta)$.

give waveplate settings for an arbitrary state, thus proving our ansatz. The operators that represent the action of half- and quarter-waveplates, respectively, are the Jones matrices [4]

$$\mathbf{O}_{HWP}(\theta) \equiv \begin{pmatrix} -\cos 2\theta & -\sin 2\theta \\ -\sin 2\theta & \cos 2\theta \end{pmatrix} \tag{6}$$

and

$$\mathbf{O}_{QWP}(\theta) \equiv \begin{pmatrix} 1-(1+i)\cos^2\theta & -(1+i)\sin\theta\cos\theta \\ -(1+i)\sin\theta\cos\theta & 1-(1+i)\sin^2\theta \end{pmatrix}, \tag{7}$$

where in each case the parameter $\theta$ is the angle the optic axis makes with horizontal.

To create arbitrary states as in (3), we start with photons in the state $\rho_H$, and direct them through a half-waveplate at $\theta_1$, giving

$$\rho_{\mathbf{1}} \equiv \mathbf{O}_{HWP}(\theta_1)\rho_H\mathbf{O}_{HWP}(\theta_1)^\dagger = \begin{pmatrix} \cos^2 2\theta_1 & \cos 2\theta_1 \sin 2\theta_1 \\ \cos 2\theta_1 \sin 2\theta_1 & \sin^2 2\theta_1 \end{pmatrix} = |2\theta_1\rangle\langle 2\theta_1|, \tag{8}$$

i.e., the pure linear polarization state $|2\theta_1\rangle$. As shown in the first box in Fig. 1, this operation is described on the Poincaré sphere by rotating the state $|H\rangle$ by 180° about an axis – representing the optic axis of the waveplate – that lies $2\theta_1$ away on the equator; the factor of 2 arises because $|V\rangle$ lies on the *opposite* side of the Poincaré sphere, i.e., 180° away from $|H\rangle$.[c]

The next step is to introduce decoherence by separating the horizontal and vertical polarization components by an optical path length difference much longer than the coherence length of the photons (see Appendix A) [6]. If the coherence length is longer than a few millimeters, one can use a polarization-dependent delay line, as shown in the second box of Fig. 1. For our downconversion source, interference filters at the detector typically define the spectral bandwidth; for filters with 10-nm full width at half maximum, the coherence length is only 49-$\mu$m. In this case it suffices to use a thick birefringent element [e.g., 1 cm of quartz] to completely decohere the polarizations within the eigenbasis of the decohering element [6]. We can control the *amount* of decoherence by tuning the polarization of the input state. For example, if the polarization before entering the decoherer is $|H\rangle$ (or $|V\rangle$) then the state purity is preserved; if the input state is diagonally polarized, i.e., $|D\rangle$, the resulting state is completely mixed. An arbitrary value of $|\vec{\mathbf{r}}|$ is produced by setting the orientation of the first half-waveplate to $\theta_1 = \frac{1}{4}\arccos|\vec{\mathbf{r}}|$. After the rotated light is directed through the birefringent decohering element, the reduced density matrix describing only the polarization is of the form (see Appendix A):

$$\rho'_{\mathbf{1}} = \begin{pmatrix} \cos^2 2\theta_1 & 0 \\ 0 & \sin^2 2\theta_1 \end{pmatrix}. \tag{9}$$

Next, using waveplates, we unitarily transform (9) into the desired final state. Note that (9) can be rewritten as an incoherent sum of a horizontally polarized pure state and an unpolarized, completely mixed state:

$$\rho'_{\mathbf{1}} = \cos 4\theta_1 |H\rangle\langle H| + 2\sin^2 2\theta_1 \rho_{mixed}\,, \tag{10}$$

where $\rho_{mixed} \equiv \frac{1}{2}\mathbf{I}$ is the completely mixed state. Because quantum mechanics is linear, we may operate individually on each part of this sum to realize the final state. As the unpolarized

[c] A very complete discussion of the use of the Poincaré sphere to describe the action of various crystal optics may be found in [5].

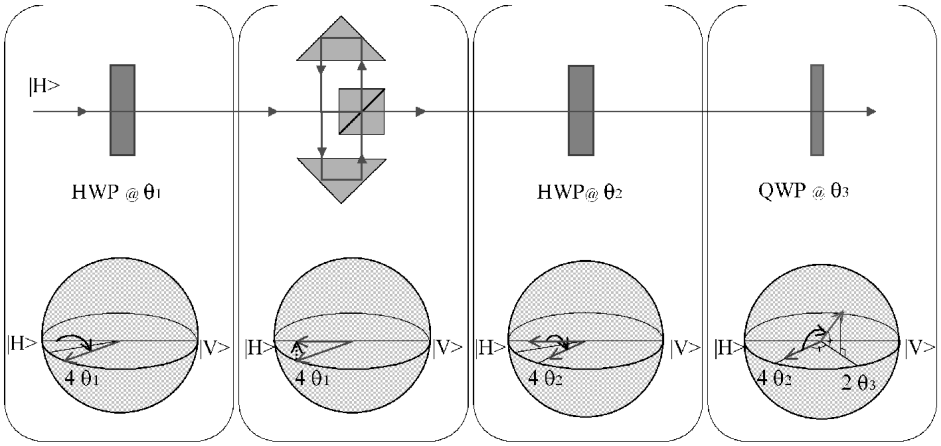


Fig. 1. The experimental setup to realize an arbitrary single (polarization) qubit, along with the representation of the state in the Poincaré sphere at each step of state preparation. In the first stage, on the left, horizontally polarized photons are sent through a half-waveplate (HWP) with an optic axis at $\theta_1$ from horizontal, giving the linear polarization state $|2\theta_1\rangle$. This is then sent through a decoherer that has an optical path length difference greater than the coherence length of the photon. One method to achieve such a decoherer is with a polarizing beamsplitter that sends vertical polarization in a delay loop while horizontal is transmitted, thereby suppressing the phase coherence in the horizontal-vertical basis (see Appendix A), and eliminating any amplitude in the off-diagonal elements of the state. Decoherence in the Poincaré sphere appears as a projection of the state onto the $|H\rangle - |V\rangle$ "spindle" (second box). By appropriately adjusting the first HWP, states with arbitrary mixedness can be produced, ranging from a pure state ($|\vec{\mathbf{r}}| = 1$) to a completely mixed state, i.e., unpolarized photons. The last two waveplates, a HWP and a quarter-waveplate (QWP), set the final direction of the (possibly mixed) state on the sphere.

part is is unchanged by any unitary transformation, the final form of the state is determined by operating on the $|H\rangle\langle H|$ term with a half-waveplate (at $\theta_2$) and a quarter-waveplate (at $\theta_3$). Algebraically determining the desired values of $\theta_2$ and $\theta_3$ to obtain a particular final state is non-trivial. However, by noting the geometric action of these waveplates on the Poincaré sphere (see the third and fourth boxes of Figure 1), one can arrive at the following final solutions for the waveplate angles[d,e]:

$$\theta_1 \quad = \quad \frac{1}{4}\arccos[\sqrt{(2A-1)^2+4B^2}] \tag{11}$$

[d]In terms of the Poincaré sphere vector $\vec{\mathbf{r}}$, we have

$$\begin{aligned}
\theta_1 &= \frac{1}{4}\arccos\left(|\vec{\mathbf{r}}|\right) \\
\theta_2 &= \frac{1}{4}\left[\arctan\left(\frac{r_D}{r_H}\right) + \arctan\left(\frac{r_R}{\sqrt{r_H^2+r_D^2}}\right)\right] \\
\theta_3 &= \frac{1}{2}\arctan\left(\frac{r_D}{r_H}\right).
\end{aligned}$$

[e]In any real system, the various waveplates may have slight errors in their retardations. Nevertheless, we have shown that any single qubit state may be produced, as long as the QWP retardance error is smaller than the HWP retardance error. In this case, however, we must numerically search for the optimal waveplate settings.

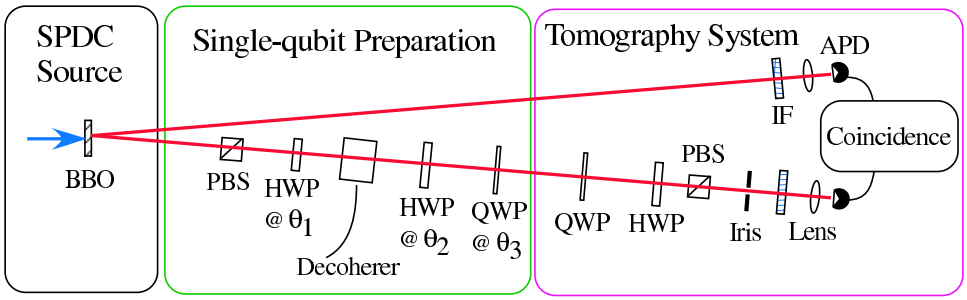


Fig. 2. Single-qubit downconversion experiment. Detection of a photon in the upper arm conditionally prepares a single-photon state in the lower arm. The polarizing beamsplitter (PBS) after the nonlinear BBO crystal prepares an extremely pure initial state $|H\rangle$, which is then transformed by the waveplates and decoherer (∼1 cm quartz birefringent element). The tomography system allows an accurate measurement of the resulting density matrix $\rho$ (see Sect. 3).

$$\theta_2 = \frac{1}{4}\left[\arctan\left[\frac{2B\cos[\delta]}{2A-1}\right] + \arctan\left[\frac{2B\sin[\delta]}{\sqrt{(2A-1)^2+4B^2\cos^2[\delta]}}\right]\right] \quad (12)$$

$$\theta_3 = \frac{1}{2}\arctan\left[\frac{2B\cos[\delta]}{2A-1}\right]. \quad (13)$$

Armed with these equations we set up our experiment as in Figure 2. The process of spontaneous parametric downconversion conditionally prepares single-photon input states [2]. A nonlinear crystal (BBO) is pumped with a vertically polarized 351-nm beam from an Argon-ion laser (average power 86 mW). The BBO is cut to produce non-collinear frequency-degenerate horizontally polarized photon pairs at 702 nm via type-I phase matching. The non-collinear photon pairs are collected in two modes, separated by 6° outside of the crystal. The first mode impinges onto a detector assembly consisting of a 10-nm FWHM interference filter (IF) centered at 702.2 nm, a lens, and an avalanche photodiode (APD) operated in Geiger mode (Perkin-Elmer #SPCM-AQR-14). Single-photon Fock states are prepared in the second arm conditional on a "trigger" count in the first detector [2]. The second mode passes through a polarizing beamsplitter (PBS) (to ensure a good fiducial state $|H\rangle$), the state preparation waveplates[f] and decoherer (1 cm quartz slab) discussed above, a QWP-HWP-PBS combination for state analysis (see Sect. 3), a 2.2-mm iris, and a detector assembly identical to that in the first mode.

We created a variety of single qubit states using this system. Some sample reconstructed density matrices are shown in Figure 3. One measure of our ability to accurately prepare specific states is the fidelity[g] between the measured and the target states. We typically observed fidelities better than 0.997; this number is presently limited by counting fluctuations due to Poisson statistics, and also to small drifts (less than 0.5%) in either the pump laser intensity or the detector efficiencies. For the data in Fig. 3, a total ∼150,000 counts were accumulated for each state.

[f] All of the waveplates are in motor-controlled stages, and can be set with an accuracy of less than 0.1°.

[g] The fidelity is a measure of state overlap [7]. For two pure states, $|\psi_1\rangle$ and $|\psi_2\rangle$, the fidelity is simply $F(|\psi_1\rangle,|\psi_2\rangle) \equiv |\langle\psi_1|\psi_2\rangle|^2$, while for two general density matrices, $\rho_1$ and $\rho_2$, the fidelity is $F(\rho_1,\rho_2) \equiv |Tr(\sqrt{\sqrt{\rho_1}\rho_2\sqrt{\rho_1}})|^2$.

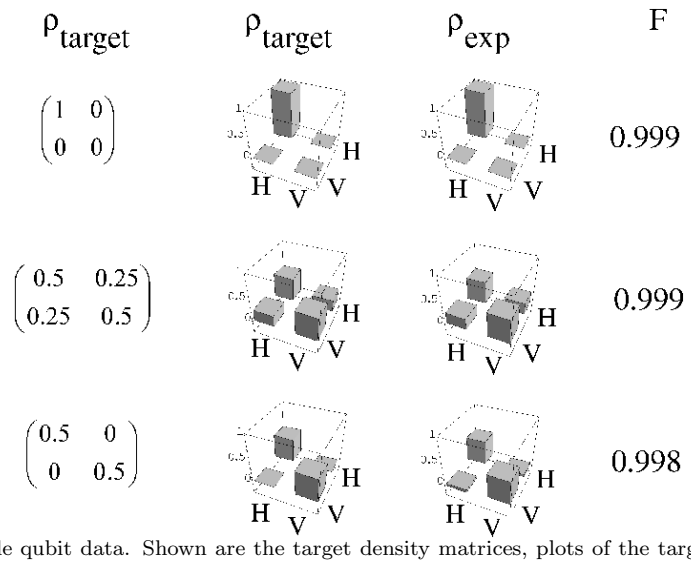


Fig. 3. Single qubit data. Shown are the target density matrices, plots of the target and experimentally measured density matrices, and the fidelity (F) between them. The imaginary elements of the density matrices are not shown because they have zero amplitude for the target states, and are always less than 2% for the experimental states.

## 3 State Characterization

One cannot determine the unknown polarization state of a photon with a single measurement. Instead, a large ensemble of photons prepared in an identical manner must be projected into different polarization basis states. Four measurements are needed – three to determine the relative values of the three independent parameters that characterize an unknown state, and a fourth to determine normalization. The polarization analysis is carried out setting the quarter- and half-waveplates shown in the tomography system box of Fig. 2. Although there are many choices as to the particular measurements that can be made (in principle measuring along any three non-collinear bases suffices), we choose the analysis states: $\langle\psi_0| \equiv \langle V|$, $\langle\psi_1| \equiv \langle H|$, $\langle\psi_2| \equiv \langle D|$, and $\langle\psi_3| \equiv \langle R|$ corresponding to $N_0$, $N_1$, $N_2$, and $N_3$ photon counts in some fixed measurement time interval (typically 100 s). As explained earlier, to obtain single photon Fock states, we count in coincidence; thus, $N_i$ are coincidence counts between the two detectors shown in Fig. 2. Since we need to estimate probabilities, we must measure a complete basis to normalize the photon counts. As $|H\rangle$ and $|V\rangle$ form a basis, $\mathcal{N} \equiv N_0 + N_1$ gives a convenient normalization factor for the $r_i$: $r_H = 2N_1/\mathcal{N} - 1$, $r_D = 2N_2/\mathcal{N} - 1$, and $r_R = 2N_3/\mathcal{N} - 1$. The density matrix of the state may then be reconstructed as in (4).

Unfortunately, as this state reconstruction is based on photon counting, statistical fluctuations or drift often yield an unphysical result; therefore, we employ a maximum likelihood technique to estimate a physical density matrix that would most likely produce the measured data. James et al. describe the technique for determining the joint state of *two* qubits [8]. Here we distill their argument down to the one qubit case (if states other than single-photon states are used, more sophisticated methods must be used to determine the quantum polarization state [9]).

A physical density matrix representation has three cardinal properties: normalization,

positive semidefiniteness, and hermiticity. Therefore, we first guess a density matrix that by definition has the aforementioned properties. A matrix that can be written as $\mathbf{T}^\dagger\mathbf{T}$ is positive semidefinite and hermitian [8]. To normalize such a matrix, we divide by its trace so that $\mathbf{T}^\dagger\mathbf{T}/Tr(\mathbf{T}^\dagger\mathbf{T})$ has the three properties for a legitimate physical density matrix. We choose the following invertible form for $\mathbf{T}(\mathbf{t})$:

$$\mathbf{T}(\mathbf{t}) \equiv \mathbf{T}(t_1, t_2, t_3, t_4) \equiv \begin{pmatrix} t_1 & 0 \\ t_3 + it_4 & t_2 \end{pmatrix}. \tag{14}$$

Using (14), the density matrix formula is

$$\rho_p(t_1, t_2, t_3, t_4) = \mathbf{T}^\dagger(\mathbf{t})\mathbf{T}(\mathbf{t})/Tr(\mathbf{T}^\dagger(\mathbf{t})\mathbf{T}(\mathbf{t})). \tag{15}$$

Next we will introduce a likelihood function that quantifies how similar $\rho_p(t_1, t_2, t_3, t_4)$ is to our experimental data:

$$\mathcal{L}(N_0, N_1, N_2, N_3; t_1, t_2, t_3, t_4) = \sum_{\nu=0}^{3} \frac{[\mathcal{N}\langle\psi_\nu|\rho_p(t_1, t_2, t_3, t_4)|\psi_\nu\rangle - N_\nu]^2}{2\mathcal{N}\langle\psi_\nu|\rho_p(t_1, t_2, t_3, t_4)|\psi_\nu\rangle}, \tag{16}$$

where the quantity $\mathcal{N}\langle\psi_\nu|\rho_p(t_1, t_2, t_3, t_4)|\psi_\nu\rangle$ represents the expected number of counts for a projection of our trial density matrix $\rho_p$ onto the analysis state $|\psi_\nu\rangle$. Note that the coincidence counts are subtracted from $\mathcal{N}\langle\psi_\nu|\rho_p(t_1, t_2, t_3, t_4)|\psi_\nu\rangle$ so that the likelihood function must be *minimized* to obtain the set of $t_i^{(opt)}$, and therefore the state that best retrodicts the actual measurements.[h]

The question of how many different states can be reliably *produced* is limited by how many may be reliably experimentally *distinguished*.[i] To determine the number of accessible distinguishable states in our system, several states in different parts of the Poincaré sphere (with approximate $|\vec{\mathbf{r}}|$ values of 0, 0.25, 0.5, 0.75, and 1) were created and measured 10 times each. We measured for 10 minutes per tomography yielding 300,000 counts per state reconstruction. For each set of measurements the average state vector $\hat{\vec{\mathbf{r}}}$ was determined. Next, the standard deviation of the ten trials was determined for three directions: $\hat{\vec{\mathbf{r}}}$, and two directions transverse to $\hat{\vec{\mathbf{r}}}$. Assuming a Gaussian distribution along these directions, we calculate that an ellipsoid with semi-axes equal to 1.69 times these standard deviations will account for over 95% of the events. These uncertainty ellipses are mainly due to count fluctuations from laser and detector efficiency drift, as well as intrinsic Poissonian counting statistics. One unexpected result of our measurements was that the thickness of the ellipsoid, i.e., the length of the minor axis along the direction of $\hat{\vec{\mathbf{r}}}$, depended on the radial coordinate $|\hat{\vec{\mathbf{r}}}|$, and varied from a minimum value of 0.0021 for $|\hat{\vec{\mathbf{r}}}| = 1$, to a maximum value of 0.0062 for

[h] The minimization is performed using the MATLAB R12 function fminunc which requires an initial estimate for the $t_i$. For the initial estimate, starting guesses for the $\rho_i$ are calculated from the measured counts $N_0$, $N_1$, $N_2$, and $N_3$; through (4), this gives a starting estimate for $\rho$, which, from (14) and (15), yields starting values for the $t_i$: $t_1 = 1 - \sqrt{1 - \frac{1}{2(1-r_H)}((1-r_H)^2 + r_D^2 + r_R^2)}$, $t_2 = \frac{\sqrt{2(1-r_H)}}{2}$, $t_3 = \frac{r_D}{\sqrt{2(1-r_H)}}$, and $t_4 = \frac{r_R}{\sqrt{2(1-r_H)}}$.

[i] When specifying a produced quantum state, it is an interesting question whether one should give an error ball (e.g., a patch on the surface of the sphere for a pure state), or simply average over this ball to yield a slightly mixed state. The former approach accounts for the fact that the error ball could shrink if more data were taken. The latter method acknowledges that the density matrix already encodes the totality of our knowledge, based on our measurements on identically prepared members of an ensemble.

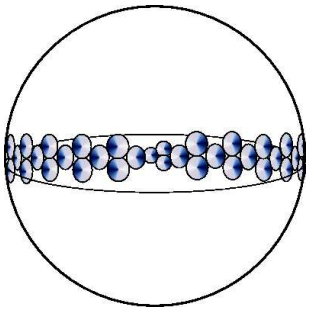

Fig. 4. Filling the Poincaré sphere with experimentally determined uncertainty "patches". These arise primarily due to counting fluctuations, either from the Poisson statistical uncertainties in photon counting, or from slight drifts ($< 0.5\%$) in the laser power or detector efficiencies. The measured uncertainty patches are approximately ellipsoids (pancakes) as shown above; for clarity their dimensions are shown scaled up by a factor of 5. Note that the thickness of the pancakes depends somewhat on the mixture of the state, indicating that some regions of the Poincaré sphere are more sensitive to counting statistics. The size of uncertainty patches implies that we are able to distinguish more than three million unique single-qubit states, assuming $\sim$10 minutes data collection time per state, i.e., $\sim$300,000 detection events).

$|\hat{\vec{\mathbf{r}}}| = 0.25$ (see Figure 4). Numerical simulations support this observation. Taking into account the varying size of the uncertainty patches, and assuming an approximate close packing of the entire Poincaré sphere volume, we estimate that we can reliably distinguish over three million states.

## 4 State Manipulation

In order to gain total control over a single qubit, it is necessary to have an understanding of what operations are physically possible. Any physical process acts as a map from all possible input states to a transformed set of output states. For example, the identity process maps every possible input state to itself. In other words, it has no effect on any input states. Other familiar processes include the unitary transformation, which when viewed in the geometric picture of the Poincaré sphere, is simply a rotation around a fixed axis (Fig. 5a); projections which either partially or completely project a state into a single basis (a single point on the Poincaré sphere, see Fig. 5b); or (partial) decoherence, which partially or completely collapses all states to the "spindle" formed by the eigenstates of the decohering interaction (Fig. 5e).

Note that while some processes, such as the identity, projection, or the unitaries, can be represented by a single 2 by 2 matrix (which operates on a two element column vector representing the qubit, as in Jones calculus), some more complex processes such as decoherence or incoherent partial polarization require a different method of characterization. Consider a simple operation (e.g., unitary or projecting) $E$ acting on a general state $\rho_{in}$. The output state is given by

$$\rho_{out} = E\rho_{in}E^{\dagger}. \tag{17}$$

A general operation $\mathcal{E}$ cannot be represented using a single $E$ matrix, but instead can be

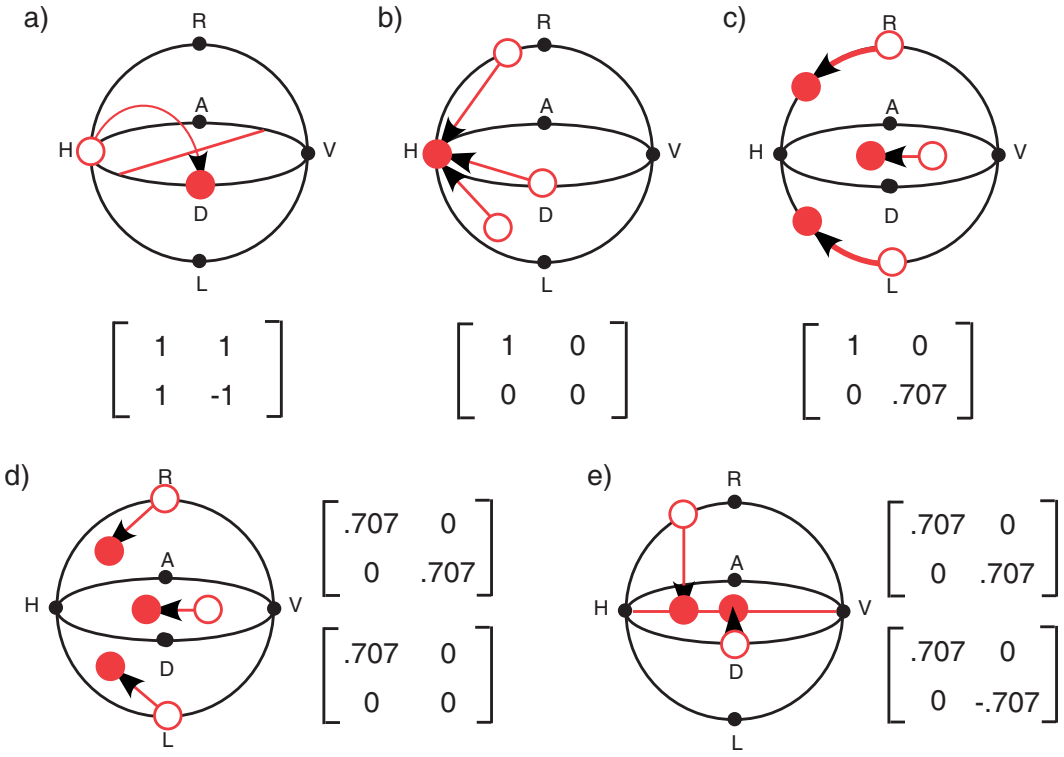


Fig. 5. Shown are several example single-qubit quantum processes. Each process is represented by both a geometric picture and by operator matrices. The geometric picture shows initial states (white balls) on the Poincaré sphere mapped to final states (solid balls). The effect of a process $\mathcal{E}$ on an input state can be defined as $\mathcal{E}(\rho_{in}) = \sum_j E_j \rho_{in} E_j^\dagger$. The operator matrices shown correspond to the $E_j$ matrices. (a) An example of a unitary transform. This transform, the Hadamard gate, corresponds to a 180° rotation about the 22.5° axis. (b) A total projection operator. This corresponds to a perfect horizontal polarizer. (c) A coherent partial polarizer. This partial projection corresponds to a device which transmits all horizontal light and half of vertical light. These two components maintain their phase relationship. Note that pure input states remain pure while all states travel towards H on the sphere. (d) An incoherent partial polarizer. This corresponds to an operation which 50% of the time projects into the H basis and 50% of the time does nothing. The photons which are subjected to the first operation are incoherently added to those of the second operation; thus this process transforms pure input states into mixed states. (e) A decoherer. This operation decoherers in the H-V basis, removing the phase relationship between these two components. All states travel in a straight line to the spindle connecting the H and V states.

described using the following operator-sum decomposition [1]

$$\rho_{out} = \mathcal{E}(\rho_{in}) = \sum_j E_j \rho_{in} E_j^\dagger. \tag{18}$$

An arbitrary number of $E$ operators can be used to represent a process, and as we saw above, decohering and partially polarizing processes require at least two matrices. The necessity of multiple $E$ operators hints at the variety of processes which must be possible, and the subtlety involved in representing an arbitrary process. Consider, for example, the partial polarizers shown in figures 5c and 5d. Figure 5c shows a coherent partial polarizer, which acts as a partial projector. Only a single $E$ matrix is necessary to represent it. Experimentally, this projector is implemented using a series of tilted glass plates for which $T_V/T_H$ is 0.5[j] All of the vertical light which passes through the glass plates maintains a definite phase relationship with all of the horizontal light which passes through. For this reason we call this a *coherent* partial polarizer.

Now consider a process which totally projects into the horizontal basis, but only acts on 50% of the measured qubits (photons). The light passing through the polarizer has no phase relationship with the light that does not, and an incoherent mixture results. We call this process an *incoherent* partial polarizer (Fig. 5d). In fact, any process which transforms a pure state into a mixed state must be represented by having one $E$ operator acting on a certain percentage of qubits, and a separate operator or operators acting on the remaining qubits. Decoherence acts in exactly this way. For example, consider the case in which the input qubits are randomly and incoherently subjected to either a $\sigma_z$ rotation (in the H-V basis) or the identity matrix. Combining the photons from the first process with those from the second, we see that any coherence between the H and V bases has been destroyed, collapsing output states to the H-V spindle on the Poincaré sphere. This action is illustrated in Fig. 5e.

Using equation (18), we can simplify the general representation of a process. First consider that the $E$ operators above can be expanded into a linearly independent basis of 2x2 operators, such as the identity matrix ($\sigma_0$) and the Pauli matrices ($\sigma_1, \sigma_2, \sigma_3$):

$$E_j = \sum_{i=0}^{3} c_i \sigma_i. \tag{19}$$

Substituting into equation (18) and combining terms,

$$\mathcal{E}(\rho_{in}) = \sum_{i,j=0}^{3} \sigma_i \rho_{in} \sigma_j \chi_{ij}. \tag{20}$$

The $\chi_{ij}$ matrix [10], a 4x4 positive Hermitian complex number matrix, shares many similarities with a state density matrix $\rho$. (For an earlier, alternate characterization of quantum processes, see [11]). While a density matrix shows the coherent and incoherent combinations of four orthogonal state vectors that make up a state, the $\chi$ matrix shows how an arbitrary process is represented by coherent and incoherent combinations of four 2x2 operators (e.g., the $\sigma$ matrices). In the case of the density matrix, a basis change can yield the same state

[j] When the plates are tilted so that the photons are incident at Brewster's angle 56° [3], the p-polarization is completely transmitted while the s-polarization suffers a reflective loss of 15% per air-glass interface.

written in a different orthogonal four-element basis. There is an exact analog to this orthogonality condition for the $\chi$ matrix, with orthogonality defined as $Tr(E_1 E_2) = 0$. In fact, if the $\chi$ matrix is diagonalized, it becomes clear that an arbitrary process can be represented by the operator-sum decomposition above, with only four orthogonal 2x2 operators in the sum. Note that in general these four operators will *not* simply be the Pauli matrices $\sigma_i$.

A physical picture of this representation corresponds to four different orthogonal 2x2 operators, each of which has a specific *probability* to act on an input qubit, i.e., they are applied incoherently. In this way an ensemble of identical input pure states can be transformed into a mixed output ensemble (see Fig. 6).

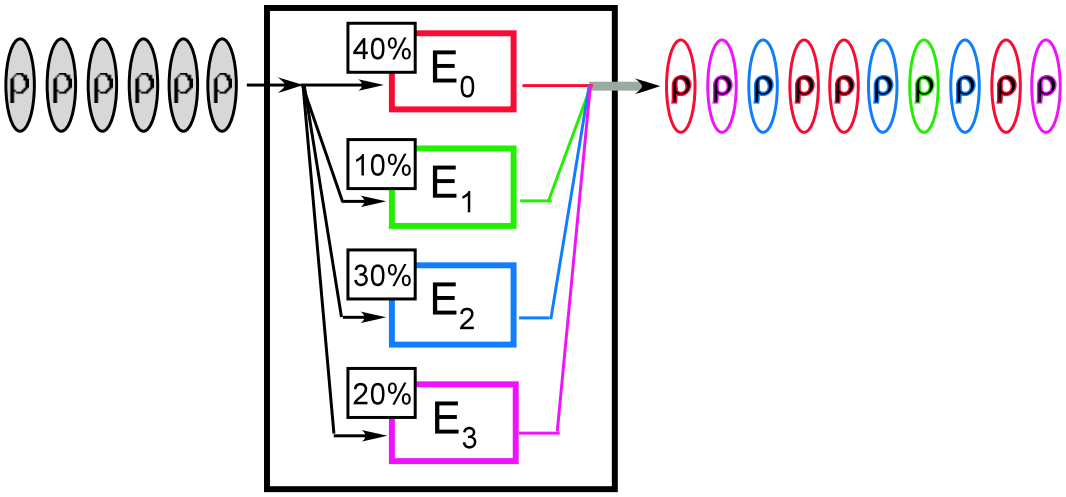


Fig. 6. An ensemble of single qubits are operated upon by an example of an arbitrary process. In general, any process can be represented by four orthogonal 2x2 operators, each of which has some percentage chance of affecting an input qubit. These four operators have no restrictions, but they must in some way incoherently act upon input qubits. In this way input pure states affected by more than one operator can be transformed into a mixed ensemble.

Now that we have a useful representation of arbitrary processes and a physical interpretation of that representation, it is necessary to be able to measure and reconstruct a given unknown process. The measurement of an unknown process is accomplished using quantum process tomography. The simplest way to measure a process involves preparing a complete basis of four single-qubit input states (e.g., H, V, D, R), subjecting each of these to the unknown process, and measuring the four output states. This is referred to as standard quantum process tomography (SQPT) [10, 11]. While this is effective, it requires four input states. It is possible, however, with a single *2-qubit* input state to exactly characterize an unknown process [12, 13, 14]. By using a second ancillary qubit, highly correlated with the primary qubit (which is subjected to the unknown process), measurements taken in coincidence on the output 2-qubit state allow reconstruction of the single-qubit process (this method is referred to as ancilla-assisted process tomography – AAPT). Because this technique requires correlation between the primary and ancillary qubits, maximally entangled states yield the most accurate AAPT results (this special case of AAPT is referred to as entanglement-assisted process tomography – EAPT). Surprisingly, there is a class of separable – completely unentangled – states which possess the necessary correlations to perform AAPT [15, 16]. All three types of

QPT have been experimentally realized: SQPT, first in NMR [17, 18] and later in photon systems [19]; EAPT [20, 21]; and AAPT using unentangled states [16]. Shown in Fig. 7 are experimental arrangements for these three techniques as demonstrated in [16].

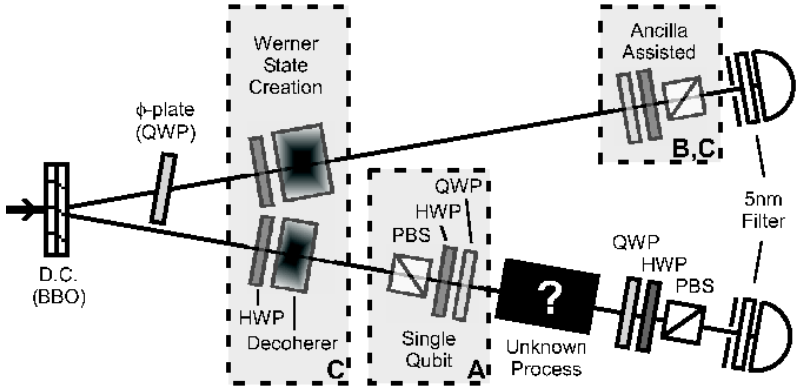


Fig. 7. Experimental setups for quantum process tomography. A, B, and C above denote which elements are present for SQPT, EAPT, and unentangled AAPT, respectively. (a) Standard quantum process tomography: Polarizer (P), half waveplate (HWP) and quarter waveplate (QWP) allow preparation of required pure single-photon states; identical elements allow tomography of the post-process states. (b) Entanglement-assisted process tomography: The source produces the maximally entangled state $(|HH\rangle - |VV\rangle)/\sqrt{2}$. A two-photon tomography of the output allows reconstruction of the process. (c) Ancilla-assisted process tomography: The source produces a separable, or completely unentangled, input state. Correlations in this state still allow AAPT.

Experimentally, we have realized a variety of processes, allowing us considerable freedom to manipulate our arbitrarily generated single-qubit states. Arbitrary unitary transformations can be generated with a series of birefringent waveplates, specifically, two quarter waveplates and a half waveplate [22]. Incoherent full or partial projection is accomplished by using polarizers, which are inserted for a fraction of the total measurement time commensurate with the strength of the desired projection. Coherent partial projection is generated using tilted glass plates. Perhaps the most interesting process, given current interest in quantum computation, is decoherence. As described in Sec. 2 and Appendix A, we introduce decoherence by passing photons through thick pieces of birefringent quartz. By varying the thickness of quartz, an arbitrary strength of decoherence can be introduced. By adding unitary transformations (waveplates) before and after the decoherer, this decoherence can be applied in any basis.

Experimentally measured processes corresponding to the theoretical examples given before are shown in Fig. 8. As before, the geometric picture offers a convenient way to visualize an otherwise complex operation. In fact, considering that an arbitrary process includes 15 independent parameters (12 to define four orthogonal 2x2 operators and 3 to assign probabilities to them), the ability to visualize its operation at all is somewhat surprising.

The natural extension of this work is toward control of multiple qubits. As this work shows, in these exponentially larger Hilbert spaces it will be increasingly important to find geometric or otherwise intuitive methods to solve the much harder problems of multiple qubit creation, characterization, and manipulation.

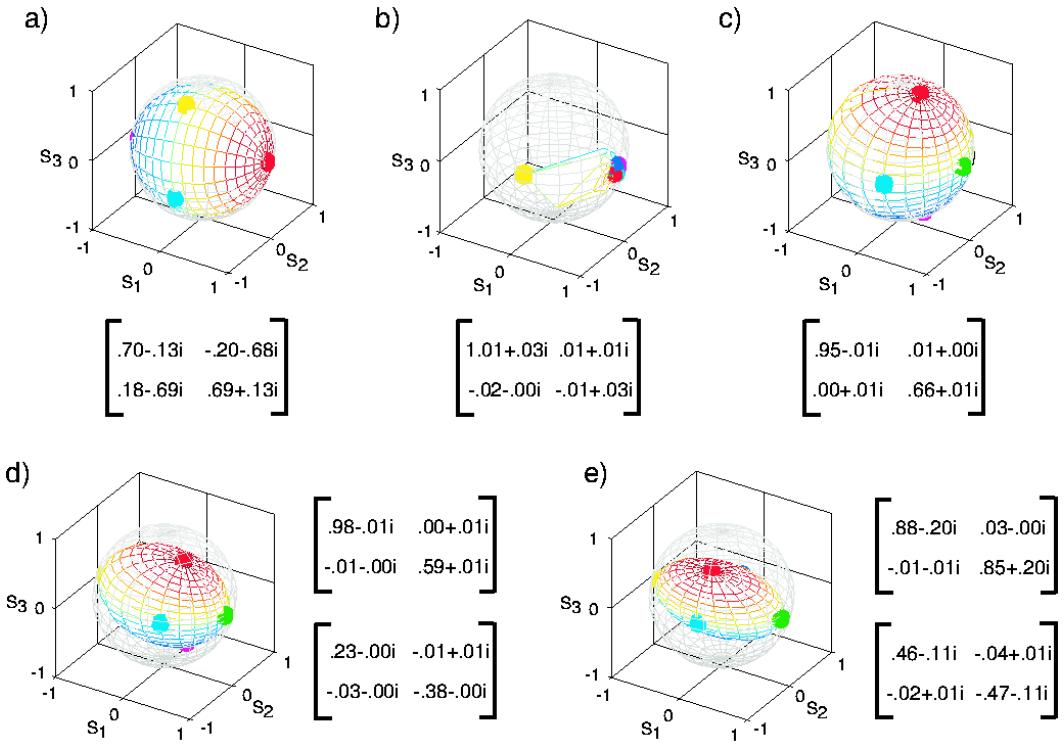


Fig. 8. Examples of experimentally generated and characterized processes are shown. The dark colored mesh corresponds to the output mapping of all input pure states. The small solid spheres correspond to the cardinal points: H (green), V(yellow), D(purple), A(blue), R(red), and L(pink). The 2x2 operator matrices correspond to the $E_j$ matrices which have a greater than 1% contribution to the measured process. Note that in contrast to the operators in Fig. 6, here we have included the probability weightings directly in the matrices shown. (a) A unitary transformation implemented using a birefringent waveplate. (b) A horizontal polarizer. Note that a single solid cardinal sphere is not mapped to H. This sphere corresponds to the vertical input case. Some small amount of vertical polarization leaks through this measured horizontal polarizer. Due to the extremely low number of vertical photons which survive this process, the experimentally calculated output state is essentially random. This highlights one disadvantage in using this geometric picture: intensity information is not directly visible. (c) A coherent partial polarizer. Implemented using tilted glass slides, this polarizer maintains the coherence of output states: thus, pure states remain pure, but slide along the surface of the sphere towards H. (d) An incoherent partial polarizer. This was simulated by inserting a horizontal polarizer into the beam 50% of the time. (e) A decoherer. A thick piece of birefringent quartz causes the H and V polarizations to separate from each other in time. They then become partially distinguishable, and pure superpositions of H and V become mixed.

## 5 Acknowledgments

We would like to thank Tzu-Chieh Wei and Daniel James for helpful discussions, and acknowledge financial support from the DCI Postdoctoral Research Fellowship Program, ARDA, and the National Science Foundation (Grant #EIA-0121568).

1. M. A. Neilsen and I. L. Chuang (2000), *Quantum Computation and Quantum Information*, Cambridge University Press (Cambridge, U. K.).

2. C. K. Hong and L. Mandel (1986), *Experimental Realization of a Localized One-Photon State*, Phys. Rev. Lett., 56, pp. 58-60.
3. M. Born and E. Wolf (1987), *Principles of Optics*, Sixth Ed., Pergamon Press (New York).
4. G. Fowles (1975), *Introduction to Modern Optics*, Second Ed., Holt, Reinhart and Winston (New York).
5. G. N. Ramachandran and S. Ramaseshan (1961), *Crystal Optics*, in *Encyclopedia of Physics*, Vol. XXV/1, edited by S. Flugge, Springer-Verlag (Berlin).
6. A. J. Berglund (2000), *Quantum coherence and control in one- and two-photon optical systems*, Dartmouth College B.A. Thesis, also quant-ph/0010001.
7. R. Jozsa (1994), *Fidelity for Mixed Quantum States*, J. Mod. Optics, 41, pp. 2315-2324.
8. D. F. V. James, P. G. Kwiat, W. J. Munroe, and A. G. White (2001), *Measurement of qubits*, Phys. Rev. A, 64, p. 052312.
9. M. G. Raymer, D. F. McAlister, and A. Funk (2000), *Quantum Communication, Computing, and Measurement '98*, Plenum (New York), pp. 147-162.
10. I. L. Chuang and M. A. Nielsen (1997), *Prescription for experimental determination of the dynamics of a quantum black box*, J. Mod. Opt., 44, p. 2455;
11. J. F. Poyatos, J. I. Cirac and P. Zoller (1997), *Complete Characterization of a Quantum Process: The Two-Bit Quantum Gate*, Phys. Rev. Lett., 78, p. 390.
12. D. Leung (2000), *Towards Robust Quantum Computation*, PhD Thesis, Stanford University, cs/0012017.
13. G. M. D'Ariano, P. Lo Presti (2001), *Quantum Tomography for Measuring Experimentally the Matrix Elements of an Arbitrary Quantum Operation* Phys. Rev. Lett. 86, p. 4195.
14. W. Dür and J. I. Cirac (2001), *Nonlocal operations: Purification, storage, compression, tomography, and probabilistic implementation*, Phys. Rev. A 64, p. 012317.
15. G. D'Ariano and P. Lo Presti (2002), *Imprinting a complete information about a quantum channel on its output state*, quant-ph/0211133.
16. J. B. Altepeter, et al. (2003), *Ancilla-Assisted Quantum Process Tomography*, Phys. Rev. Lett., 90, p. 193601.
17. M. A. Nielsen, E. Knill and R. Laflamme (1998), *Complete quantum teleportation using nuclear magnetic resonance*, Nature, 396, p. 52.
18. A. M. Childs, I. L. Chung and D. W. Leung (2001), *Realization of quantum process tomography in NMR*, Phys. Rev. A 64, p. 012314.
19. F. De Martini, G. D'Ariano, A. Mazzei and M. Ricci (2002), *Pauli Tomography: complete characterization of a single qubit device* quant-ph/0207143.
20. F. De Martini, G. D'Ariano, A. Mazzei and M. Ricci (2002), *Exploiting quantum parallelism of entanglement for a complete experimental quantum characterization of a single qubit device* quant-ph/0210210.
21. Y. Nambu et al. (2002), *Experimental investigation of pulsed entangled photons and photonic quantum channels* Proceedings of SPIE, 4917, 13.
22. Berthold-Georg Englert, Christian Kurtsiefer, and Harald Weinfurter (2001), *Universal unitary gate for single-photon two-qubit states*, Phys. Rev. A, 63, p. 032303.

## Appendix A

Decoherence always arises from the entanglement of the quantum system being considered to some other quantum degree of freedom, which is then traced over. In our system we realize decoherence by coupling the frequency and polarization degrees of freedom and then measuring in a frequency-insensitive way [6]. The state of a photon written in terms of its polarization and frequency spectrum is $|\xi\rangle = (\alpha|H\rangle + \beta|V\rangle) \otimes \int d\omega A(\omega)|\omega >$, where $\alpha$ and $\beta$ are complex normalized coefficients, and $A(\omega)$ is the complex amplitude for frequency $\omega$, normalized such that $\int d\omega |A(\omega)|^2 = 1$.

To decohere in the $|H\rangle/|V\rangle$ basis, we send the photon through a birefringent element whose fast axis is parallel to the horizontal polarization. Traversing a birefringent element of length L adds a phase that is polarization and frequency dependent, producing the state $|\xi_D\rangle = \int d\omega(e^{i\frac{n_H L}{c}\omega}\alpha|H\rangle + e^{i\frac{n_V L}{c}\omega}\beta|V\rangle)A(\omega)|\omega>$. Tracing over the frequency gives

$$|\xi_D\rangle \rightarrow \rho_D = \begin{pmatrix} |\alpha|^2 & \alpha\beta^* \int_{-\infty}^{\infty} d\omega |A(\omega)|^2 e^{i\phi(\omega)} \\ \alpha^*\beta \int_{-\infty}^{\infty} d\omega |A(\omega)|^2 e^{-i\phi(\omega)} & |\beta|^2 \end{pmatrix}, \tag{A.1}$$

where $\phi(\omega) = (n_H - n_V)\frac{L}{c}\omega$. As long as $(n_H - n_V)L$ is much greater than the photon's coherence length,[k] the off-diagonal elements of expression (A.1) will effectively average to zero, and the polarization state will be fully decohered. Note that although this form of decoherence due to dephasing is reversible (i.e., by using a compensating birefringent element), it is fundamentally no different than any other type of decoherence, which *in principle* is always reversible if one could access the entire Hilbert space describing all parts of the experiment.

[k]The coherence length ($L_c$) of the photon is determined by the Fourier transform of the spectrum $A(\omega)$. For example, if $A(\omega)$ is a Gaussian of full width at half maximum $\Delta\omega$, then $L_c = \frac{2\pi c}{\Delta\omega}$.